

CENTRAL ROTATION CURVES OF SPIRAL GALAXIES

Y. SOFUE,¹ Y. TUTUI,¹ M. HONMA,¹ A. TOMITA,² T. TAKAMIYA,¹ J. KODA,¹ AND Y. TAKEDA¹

Received 1999 February 4; accepted 1999 May 5

ABSTRACT

We present high-resolution central-to-outer rotation curves for Sb, SBb, Sc, and SBC galaxies. We discuss their general characteristics, particularly their central behavior, as well as dependencies on morphological types, activity, and peculiarity. The rotation curves generally show a steep nuclear rise and high-velocity central rotation, followed by a broad maximum in the disk and then a flat rotation due to the massive halo. Since the central high velocity and steep rise are common to all massive galaxies, they cannot be due to noncircular motions. Disk rotation curves of barred galaxies show larger dispersion than those of normal galaxies, probably because of noncircular motions. Interacting galaxies often show perturbed outer rotation curves, while their central rotation shows no particular peculiarity. In addition, central activities, such as starbursts and active galactic nuclei, appear to show no particular correlation with the property of rotation curves. This would suggest that the central activities are triggered by a more local effect than the global dynamical property.

Subject headings: galaxies: kinematics and dynamics — galaxies: nuclei — galaxies: spiral

1. INTRODUCTION

Rotation curves are the principal tool used to derive the axisymmetric distribution of mass in spiral galaxies in the first-order approximation. Rotation curves of galaxies in the disk and outer regions have been obtained based on optical and H I line spectroscopy (Rubin, Ford, & Thonnard 1980, 1982; Bosma 1981; Clemens 1985; Mathewson & Ford 1996; Persic & Salucci 1995; Persic, Salucci, & Stel 1996; Honma & Sofue 1997b). These rotation curves have been used to estimate the mass distribution in the disk and halo, particularly for the dark halo, using a model–potential fits method (e.g., Kent 1987, 1992). Persic et al. (1996) have extensively studied the universal characteristics of rotation curves in the outermost regions. However, the inner rotation curves have not yet been thoroughly investigated with sufficient accuracy, both because the concern in these studies has been the distribution of mass in the outermost regions and because of the difficulty in deriving the central rotation velocities. The difficulty in measuring central rotation curves is mainly due to the lack of H I gas in the central regions, as well as contamination from bright bulge light, when photographic plates are used.

In our recent papers, we have stressed that for deriving central rotation curves, CO molecular lines are most convenient because of the high concentration of molecular gas in the centers of many galaxies, the high angular and velocity resolutions in CO observations, and the negligible extinction even toward the nuclear dusty disk. We have thus used high-resolution CO line data to obtain well-sampled inner rotation curves for nearby galaxies (Sofue 1996, 1997; Sofue et al. 1997, 1998, hereafter Papers I to IV, respectively). Recent CCD H α line spectroscopy has also made available to us accurate rotation curves for the inner regions, as a result of the large dynamic range and the more precise subtraction of bulge continuum light for digital images, in so far as the extinction is not very large; the optical position-velocity (PV) diagrams obtained often show high-velocity

central components (Rubin, Kenney, & Young 1997; Sofue et al. 1998; Bertola et al. 1998). However, it is not yet known whether the central steep rise of rotation velocity is universal or how it is correlated with other properties of galaxies, such as the Hubble type and central activity.

In this paper, we present high-accuracy rotation curves for Sb, SBb, Sc, and SBC galaxies and discuss their general characteristics, particularly for central rotation curves. We also discuss their dependence on morphological types, activity, and peculiarity. Individual rotation curves are shown in the Appendix, and machine-readable data are available by contacting the first author. The rotation-curve data, from the central to outer regions in high accuracy, will be used to derive the detailed mass and mass-to-luminosity ratios in a separate paper (Takamiya & Sofue 1999a).

2. CENTRAL-TO-OUTER ROTATION CURVES

2.1. Milky Way

The rotation curve of the Milky Way is shown in Figure 1a, as reproduced from the literature (Clemens 1985; Honma & Sofue 1997a). Recently, it has been shown that the velocity dispersion of stars within the central 10 pc increases toward the center, indicating the existence of a massive black hole (Genzel et al. 1997; Ghez et al. 1998). Assuming the existence of a black hole of $2.6 \times 10^6 M_{\odot}$, we have calculated a corresponding rotation curve and combined it with the existing CO data to obtain a rotation curve of the Milky Way as shown in Figure 1b in a logarithmic plot. In addition to the Galaxy, evidence for nuclear massive black holes has been accumulating for many other galaxies (Miyoshi et al. 1995; Richstone et al. 1998), suggesting similar central rotation curves (see § 3.3).

Thus, the rotation curve of our Galaxy can be described as having:

1. A high-density core, including the massive black hole, which causes a nonzero velocity very close to the center.
2. A steep rise within the central 100 pc.
3. A maximum at radius about 300 pc, followed by a decline to a minimum at 2 kpc.
4. A gradual rise from 2 kpc to the disk maximum at 6 kpc.

¹ Institute of Astronomy, University of Tokyo, Mitaka, Tokyo 181-8588, Japan.

² Faculty of Education, Wakayama University, Wakayama 640-8510, Japan.

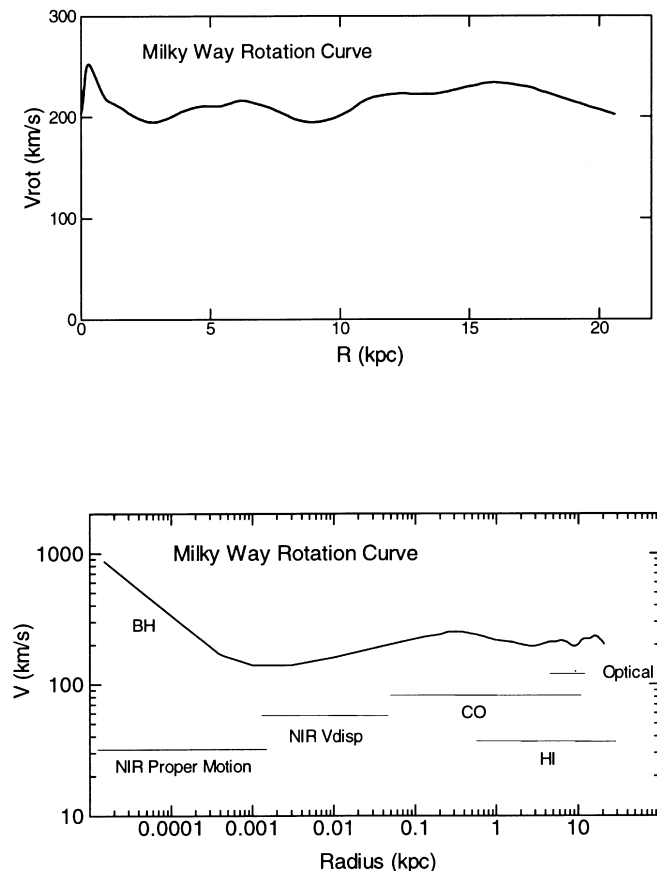


FIG. 1.—(a) Rotation curve of the Milky Way plotted in linear scale. (b) Rotation curve plotted in a logarithmic scale; this obeys the Keplerian law near the center due to the massive black hole.

5. A nearly flat outer region with a dip at 8 kpc, followed by a second maximum at 15 kpc, followed further by an outermost Keplerian decline.

2.2. Well-sampled Extended Rotation Curves

Except for the Milky Way, it has been widely believed that the central rotation curves of most galaxies behave in a rigid-body fashion. These rotation curves appear to behave differently from that of the Milky Way in the inner disk and bulge regions. The question might arise, then, whether the Milky Way really is an exception, or whether a similar rotation property is not showing up in the currently published rotation curves of galaxies.

We have performed high-resolution CO line observations of galaxies to obtain PV diagrams and combined them with existing H I and optical rotation curves. We have also obtained CCD spectroscopy in the H α and [N II] line emissions of the central regions of galaxies. We have applied the envelope-tracing method to derive rotation curves from PV diagrams. In Figure 2a we show the most completely sampled rotation curves obtained with this method for all sample galaxies (Papers I–IV), and in Figure 2b we show the same but for the central 5 kpc. Figure 2c shows some rotation curves plotted against radii normalized by the scale-length radius of the exponential disk.

In deriving rotation curves we have applied the envelope-tracing method, which traces the terminal velocities in position-velocity diagrams along the major axes, which

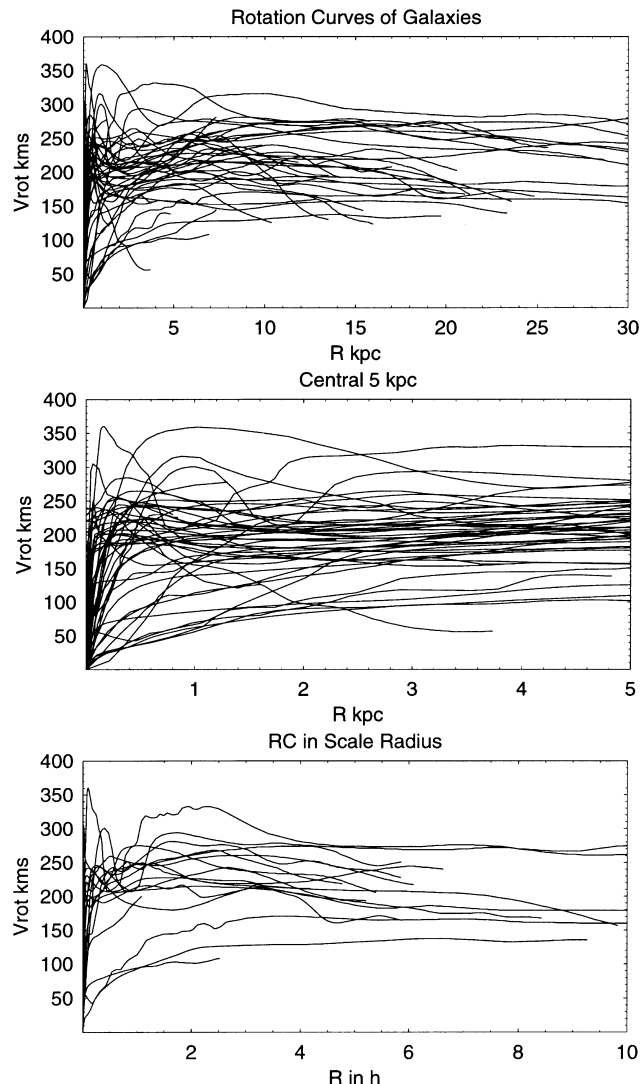


FIG. 2.—Most completely sampled rotation curves of Sb and Sc galaxies obtained using CO, H α , and H I line data. (a) All galaxies; (b) all galaxies for central 5 kpc; (c) rotation curves with radii normalized by scale radius of exponential disk.

method is described in detail in Papers I and II. This method has the advantage that it estimates the rotation velocity in the central regions more accurately than the methods used in other current analyses (e.g., Warner, Wright, & Baldwin 1973; Rubin et al. 1980; Persic et al. 1996), which gave intensity-weighted velocities (see also § 4.2).

In Figures 3a, 3b, and 3c, we show rotation curves for Sb, Sc, and barred (SBb and SBc) galaxies, respectively. Figure 4 shows rotation curves for peculiar galaxies and interacting galaxies. Individual rotation curves are published in the literature given above with detailed discussion, and displayed in Figure 10 of the Appendix. Parameters for individual galaxies are also listed in the Appendix in Table 1.

2.3. Sb Galaxies

All Sb galaxies in Figure 3a have rotation curves with a very steep rise in the central 100–200 pc region, often associated with a peak at radii $r \sim 100$ –300 pc. The rotation

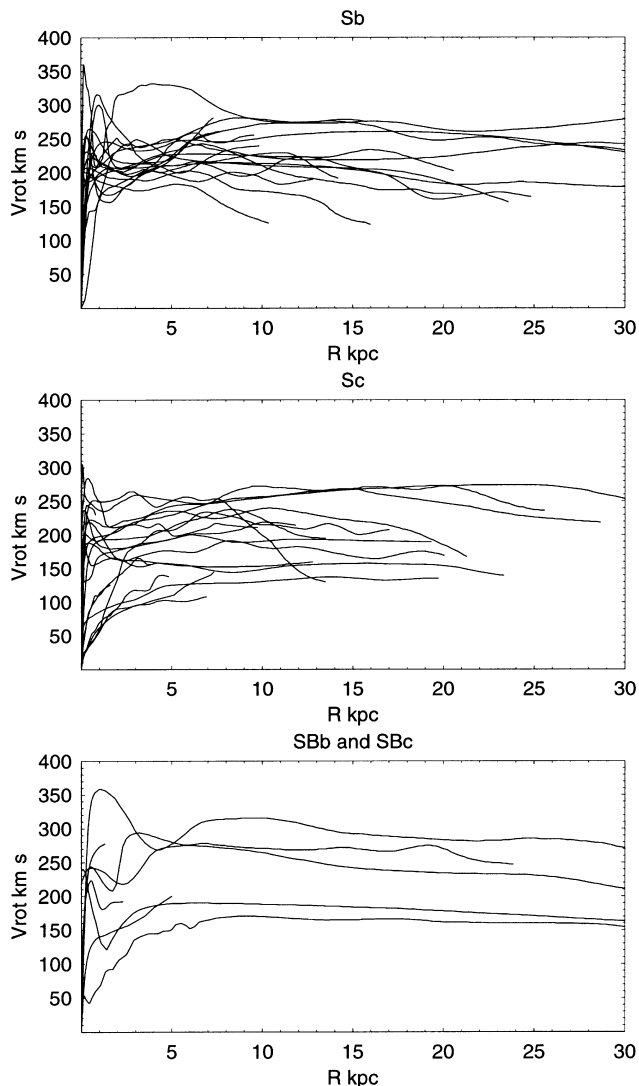


FIG. 3.—(a) Sb, (b) Sc, and (c) barred galaxies (SBb and SBc)

velocity then declines to a minimum at $r \sim 1$ kpc, followed by a gradual rise to a broad maximum at $r \sim 2\text{--}7$ kpc, corresponding to the disk. The outermost parts are usually flat, indicating the massive dark halo. Some galaxies, such as the Milky Way, show a declining outer rotation (Honma & Sofue 1997a, 1997b). Thus, the rotation curves for Sb galaxies are essentially the same as that of the Milky Way.

2.4. Sc Galaxies

Sc galaxies tend to have slower velocities than Sb, and the rotation velocities are more spread out from ~ 100 to ~ 200 km s^{-1} among the sample galaxies. Massive Sc galaxies show a steep nuclear rise similar to Sb's, while less massive galaxies have a more gentle rise. They also have a flat rotation until their outer edges.

2.5. Barred SBb and SBc Galaxies

In Figure 3 we compare barred galaxies with nonbarred galaxies. There appears to be no particular difference in their general properties: the rotation properties of the barred galaxies are almost the same as those of nonbarred

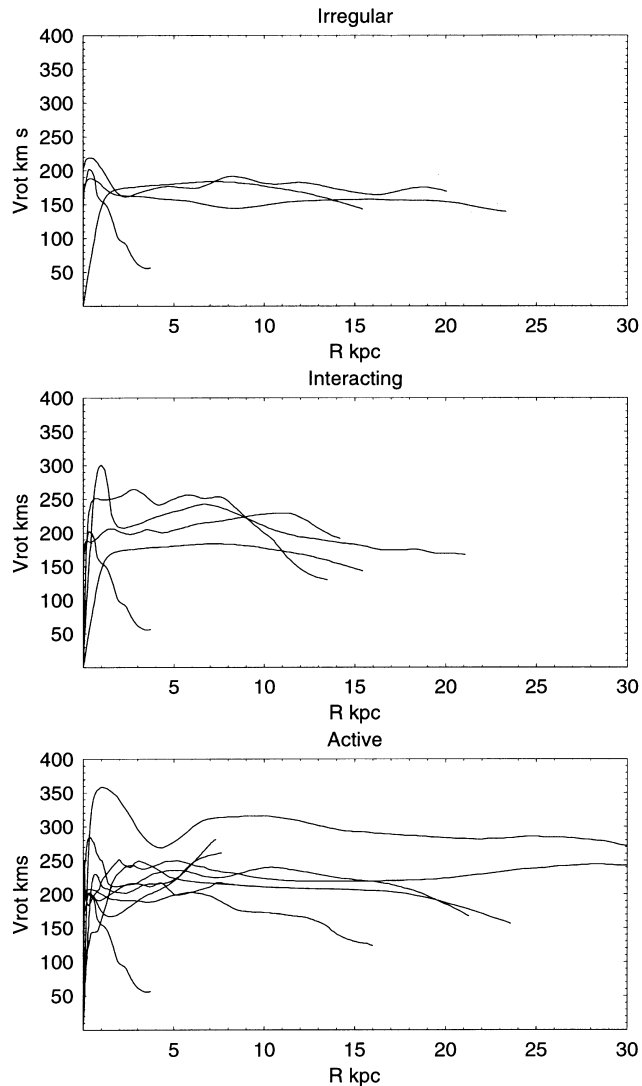


FIG. 4.—(a) Peculiar and irregular galaxies, (b) interacting galaxies, and (c) galaxies with active nuclei and/or starbursts.

galaxies of Sc and Sb types. However, barred galaxies tend to show a larger amplitude velocity variation with radius of about $\pm \sim 30\text{--}40$ km s^{-1} within the main disk at $R \sim 2\text{--}5$ kpc. The large velocity variation may be due to a barred potential of a length of several kpc. In order to clarify this and investigate the noncircular motions, two-dimensional velocity fields are necessary; these are, however, beyond the scope of this paper, and remain a future subject. On the other hand, normal galaxies usually show velocity variation of about $\pm 10\text{--}20$ km s^{-1} , mainly caused by spiral arms, except in a few cases.

2.6. Peculiar and Interacting Galaxies

Rotation curves for irregular galaxies NGC 660, NGC 3034, NGC 4631, and NGC 4945 are shown in Figure 4a. NGC 660 is a polar-ring galaxy with a warped galactic disk, while the rotation curve from the disk to outer polar ring behaves as if they are continuous structures. NGC 3034 (M82) shows a very exceptional behavior of rotation: it has a steep nuclear rise as usual, but decreases after the nuclear peak, obeying the Keplerian law. This may be the result of a

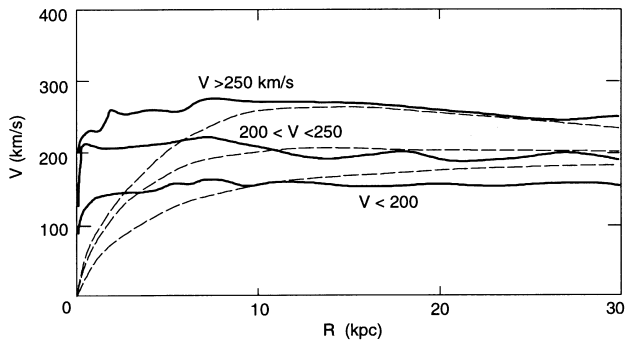


FIG. 5.—Mean rotation curves for galaxies with disk rotation velocities higher than 250 km s^{-1} (top), between 200 and 250 km s^{-1} (middle), and lower than 200 km s^{-1} (bottom). Universal rotation curves (URC) formulated by Persic et al. (1996) are shown by dashed lines for several values of galaxy luminosities.

strong tidal truncation of the disk by a close encounter with M81 (Sofue 1998). NGC 4631 is an interacting dwarf galaxy with peculiar morphology, showing a rigid-body increase of rotation velocity. Since this galaxy is edge-on, it is not clear

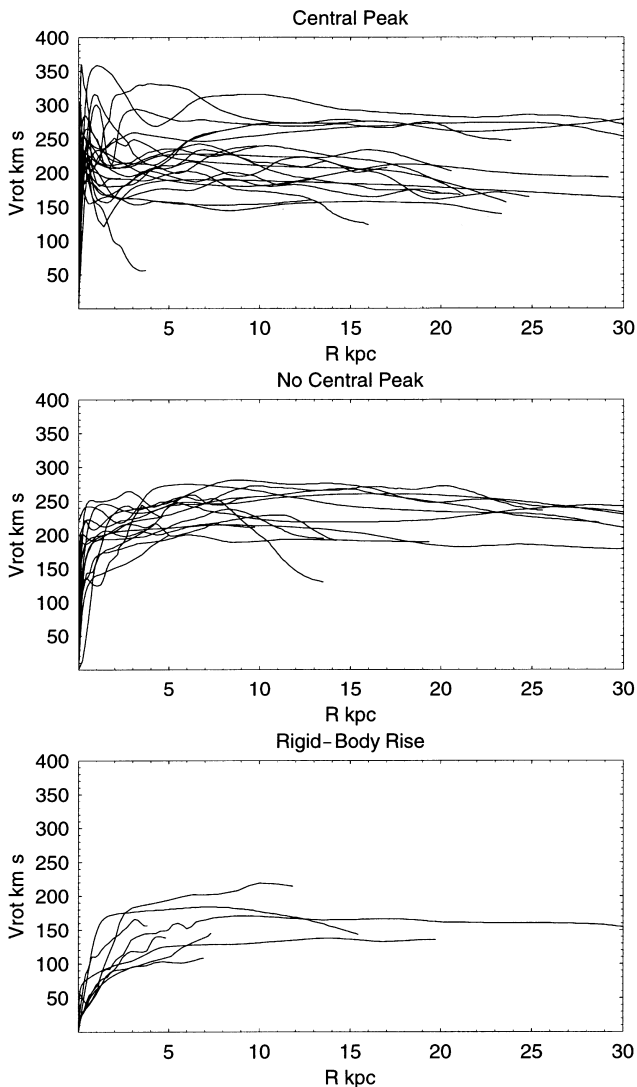


FIG. 6.—Classification of rotation curves into three types according to the central behavior.

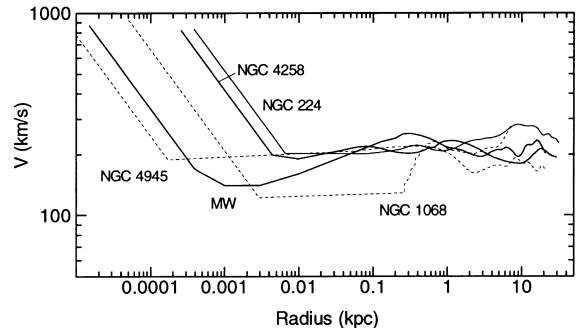
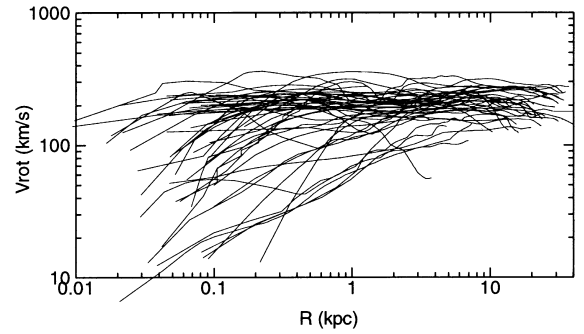


FIG. 7.—Logarithmic rotation curves for (a) all galaxies and (b) galaxies with central massive black holes.

whether the CO gas is indeed lacking in the center, or whether this effect results from a true rigid-body rotation. NGC 4945 shows peculiar dark lanes and patches, but a quite normal rotation: a steep nuclear rise and flat-disk rotation. Its peculiar distribution of interstellar gas is probably due not to its global dynamical characteristics, but to a local phenomenon in the gas disk.

The interacting galaxy NGC 5194 (M51) shows a very peculiar rotation curve (Fig. 4b; see also Fig. 10), which declines more rapidly than the Keplerian law at $R \sim 8\text{--}12$ kpc. This may be due to variation of the inclination angle with the radius, or warping. In fact, this galaxy is nearly face-on ($i = 20^\circ$), but a slight warp would cause a large error in deriving the rotation velocity; if the galaxy's outer disk at 12 kpc has an inclination as small as $i \sim 10^\circ$, such an apparently steep decrease would be observed even for a flat rotation.

2.7. Activity and Rotation Curves

Our sample includes galaxies having various activities, such as starbursts (NGC 253, NGC 1808, NGC 3034), Seyfert galaxies (NGC 1068, NGC 1097), LINERs (NGC 3521, NGC 4569, NGC 7331), and nuclear jets (NGC 3079). In Figure 4c we plot rotation curves for these galaxies. The global rotation and mass distribution appear rather normal in these active galaxies, and no peculiar behavior is found within our resolution. This implies that such activities are triggered by a more local and secondary cause rather than by a global dynamical mass distribution. An exception is the starburst galaxy NGC 3034 (M82), which shows a usual nuclear rise but followed by a Keplerian declining rotation, indicating a tidal truncation of the disk (Sofue 1998), as mentioned in § 2.6.

3. UNIVERSAL PROPERTIES

3.1. Averaged Rotation Curves

In Figure 5 we show mean rotation curves, which have been obtained by averaging rotation velocities for three mass classes: massive galaxies with a maximum disk velocity greater than 250 km s^{-1} , galaxies with maximum disk velocities between 200 and 250 km s^{-1} , and less massive galaxies with velocities less than 200 km s^{-1} . In Figure 5 we also plot the universal rotation curves (URC) formulated by Persic et al. (1996). The observed mean rotation curves at $R > 10 \text{ kpc}$ are well fitted by the URC. Since the URC has been derived specifically for studying massive halos, the disk and central rotation curves may not be well reproduced. In fact, the central rotation curve obtained in this study is much steeper than the URC. This may be partly due to the difference in the methods used to derive the rotation curve; rotation curves in previous studies have usually been derived from the intensity peak in the PV diagrams. On the other hand, in the present study we have used the envelope-tracing method, which is thought to be more reliable in tracing the central rotation curve (Sofue 1996; Takamiya & Sofue 1999b). A discussion of rotation curves and position-velocity diagrams will be given in § 4.2.

3.2. Classification of Central Rotation Curves

The observed rotation curves can be classified into the following three types, according to their behavior in the central regions. Figures 6a–6c show the classified rotation curves.

Central Peak Type.—Rotation velocity attains a sharp maximum near the center at $R \sim 100\text{--}500 \text{ pc}$, followed by a dip at $\sim 1 \text{ kpc}$, then by a broad maximum of the disk component. Examples are the Milky Way, NGC 891, NGC 3079, NGC 5907, and NGC 6946.

No Central Peak Type.—The rotation curve rises steeply at the center, followed immediately by a flat part. Examples are NGC 224, NGC 253, IC 342, NGC 5194, and NGC 5055.

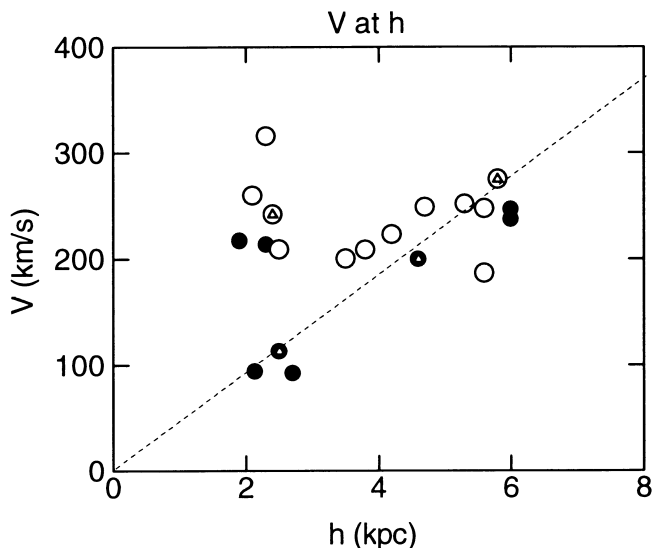


FIG. 8.—Rotation velocities at scale radius h and $2.2h$ plotted against h . Open circles represent Sb, filled circles Sc, and circles with triangles barred galaxies.

Rigid-Body Type.—The rotation velocity increases mildly from the center in a rigid-body fashion within the central 1 kpc. This type is rather the exception, and is found in less massive Sc-type galaxies, such as NGC 598, NGC 2403, NGC 3198, and NGC 4631. This tendency has been already noticed by Casertano & van Gorkom (1991).

3.3. Logarithmic Rotation Curves

Since the dynamical structure of a galaxy varies with the radius rapidly toward the center, an alternative plot of rotation curves, such as in logarithm, would help us to overview the innermost kinematics. In fact, the logarithmic plot in Figure 1b has demonstrated its convenience for discussing the central mass distribution, including the black hole of our Galaxy. In Figure 7 we plot in logarithmic scaling the same rotation curves shown in Figure 2a. The central 1 kpc regions are better presented in this figure. However, resolutions of our data are not sufficient to express rotation characteristics in the very center, particularly within 100 pc for many galaxies.

Although we must be careful in looking at this figure in the sense that the resolution is limited in the central few hundred pc, we can safely argue that high-mass galaxies show almost constant rotation velocities from the center to the outer edge, in so far as they are presented in such a logarithmic plot. On the other hand, lower mass galaxies show decreasing rotation toward the center in the central 1 kpc regions. However, we must also note that the declining rotation toward the center might be caused by insufficient angular resolution, which often causes position-velocity diagrams to miss the central steep rise.

A logarithmic rotation curve is particularly useful for such cases with central massive black holes. Figure 7b shows rotation curves of four galaxies from our sample for which the existence of massive black holes is evident (Richstone et al. 1998): NGC 4258 (Miyoshi et al. 1995), the Milky Way (Genzel et al. 1997; Ghez et al. 1998), NGC 224 (Magorrian et al. 1998), and NGC 4945 (Greenhill, Moran, & Herrnstein 1997). Here, equivalent rotation velocities corresponding to the black hole masses are plotted by tilted straight lines, obeying $V \propto R^{-1/2}$. Except for the Milky Way, they are connected to known rotation curves by horizontal straight lines in the regions where detailed observations are lacking. In these galaxies, the rotation velocity never declines to zero at the center.

3.4. Scale Radius and Disk Rotation Velocity

Maximum rotation velocity is an indicator of the total mass of a galaxy (e.g., Persic et al. 1996). The disk mass is also related to the optical scale radius (h), because the mass-to-luminosity ratio would not vary significantly inside the disk. It is interesting to see how the scale radius of a disk is correlated with the maximum velocity of rotation, which will occur at $R = 2.2h$ for an exponential disk, as can be observed in Figure 2. In Figure 8 we plot rotation velocities at $R = h$ and $R = 2.2h$ against the scale radius, h , from our sample galaxies, where open circles represent Sb, filled circles Sc, and triangles barred galaxies.

Although the correlation between velocity and scale radius is not tight, there appear to exist two types of rough correlations: (1) one group contains galaxies with rotation velocities linearly correlated with the scale radius, approximately fitted by the dashed line, while (2) another group comprises galaxies with largely scattered velocities but with

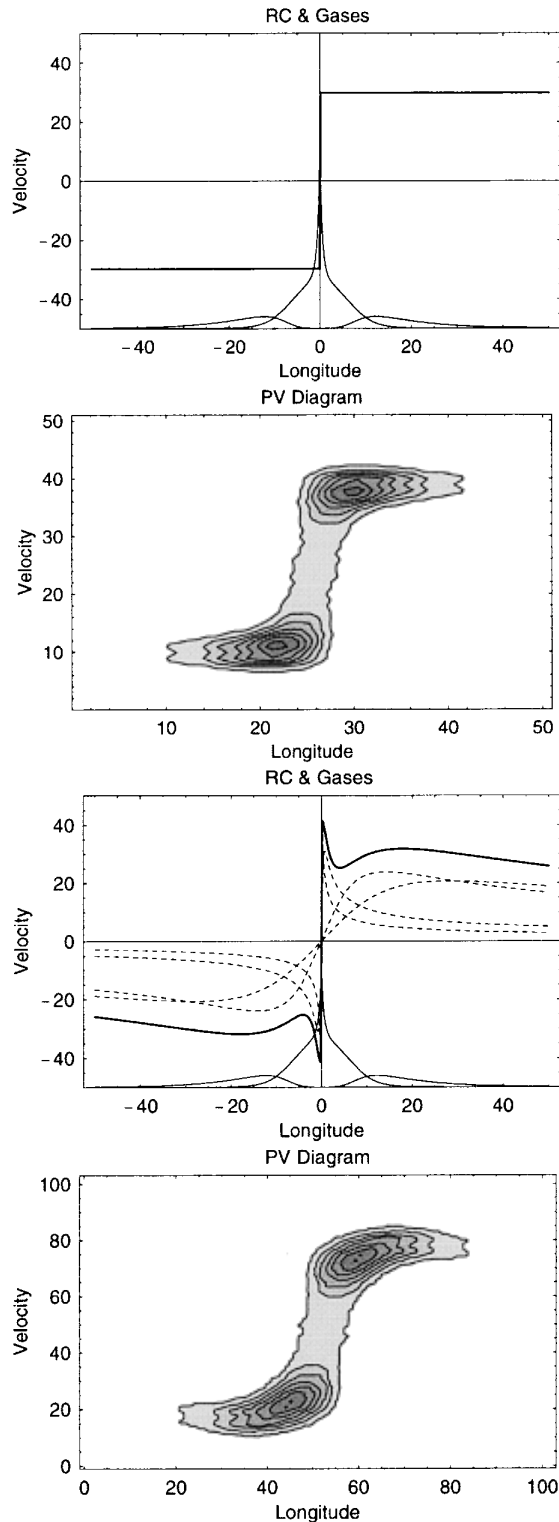


FIG. 9.—Simulation of position-velocity diagrams from assumed rotation curves and gas distribution. (a) Rotation velocity is assumed to be constant, and therefore the central velocity is finite. (b) Four mass components (core, bulge, disk, and halo) are assumed, having a very sharp central rise of rotation velocity. Note that the high velocities in the center and steep nuclear rise are hardly detected in PV diagrams with finite resolution. This simple simulation suggests that observed PV diagrams often miss a massive compact component in the center.

scale radii about constant at $h \sim 2.3$ kpc. No particular trend for barred galaxies, such as larger scatter, is found in this plot.

4. DISCUSSION

4.1. Steep Nuclear Rise and High Rotation Velocity in the Center

The extremely high frequency of massive galaxies showing the steep nuclear rise indicates that the high velocity is not due to a particular view of noncircular motion by chance. Note that the probability of looking at a bar end-on is much smaller than that of viewing one side-on, which should result in a larger probability for apparently slower rotation than circular velocity at a given radius; therefore, masses estimated from the circular assumption would be even underestimated if they contain a bar. So far as our sample galaxies are concerned, the steep nuclear rise of the rotation velocity is a universal property for massive Sb and Sc galaxies, regardless of the existence of a bar and morphological peculiarities. However, less massive galaxies tend to show a rigid-body rise.

We can summarize that the rotation curves of massive Sb and Sc galaxies, in general, comprise the following four components:

1. Steep central rise and peak, often starting from an already high velocity at the nucleus.
2. Bulge component.
3. Broad maximum by the disk.
4. Halo component.

We stress that the rotation velocities in many well-resolved galaxies do not decline to zero at the nucleus. This indicates that the mass density increases toward the nucleus more rapidly than expected from exponential or de Vaucouleurs laws. We mention that the widely adopted zero velocity in the center may be merely due to a custom of drawing a rotation curve by linking positive and negative velocities from the opposite sides of the nucleus.

4.2. High Velocities in the Center and Observed PV Diagrams

We point out that nearer galaxies with higher effective resolution in our sample tend to show steeper nuclear rise. This suggests that an even steeper central rise would be observed in more distant galaxies, if they were observed at higher resolution. In order to examine how central high velocities would appear in an observed PV diagram with finite resolution, we have simulated PV diagrams from assumed rotation curves and a model distribution of interstellar gas. Figure 9a shows a case in which the rotation velocity is assumed to be constant, so that the velocity does not decline to zero at the center, and the interstellar gas is centrally peaked. However, the calculated PV diagram shows a rigid-body behavior near the center, and if we trace the intensity peak on this PV diagram, the velocity at the center would be measured to be zero. Hence, in so far as a rotation curve constructed from a PV diagram is concerned, we should not take its central rigid body-like behavior strictly; the true velocity may be much higher, or may even start from a finite value near a central black hole.

Figure 9b shows a case with a more realistic rotation curve, comprising four components: a central compact core, bulge, disk, and massive halo, each expressed by a Plummer potential. In the calculated PV diagram, however, the central steep rise and the peaks due to the core and bulge are hardly recognized. This simulation demonstrates that tracing peak-intensity loci in observed PV diagrams could

miss possible central high velocities. We thus conclude that the central rotation curves derived from observed PV diagrams generally give *lower limits* to the rotation velocities. In fact, high-resolution central PV diagrams observed for some spiral galaxies by Bertola et al. (1998) have indicated

velocities much higher than those currently supposed, indicative of massive central black holes. Detailed discussion of PV diagrams and a method to derive more reliable rotation curves will be given in a separate paper (Takamiya & Sofue 1999b).

APPENDIX

We present rotation curves for individual galaxies in Figure 10. Machine-readable data in the form of tables are available by contacting the first author. Table 1 lists the parameters of the galaxies.

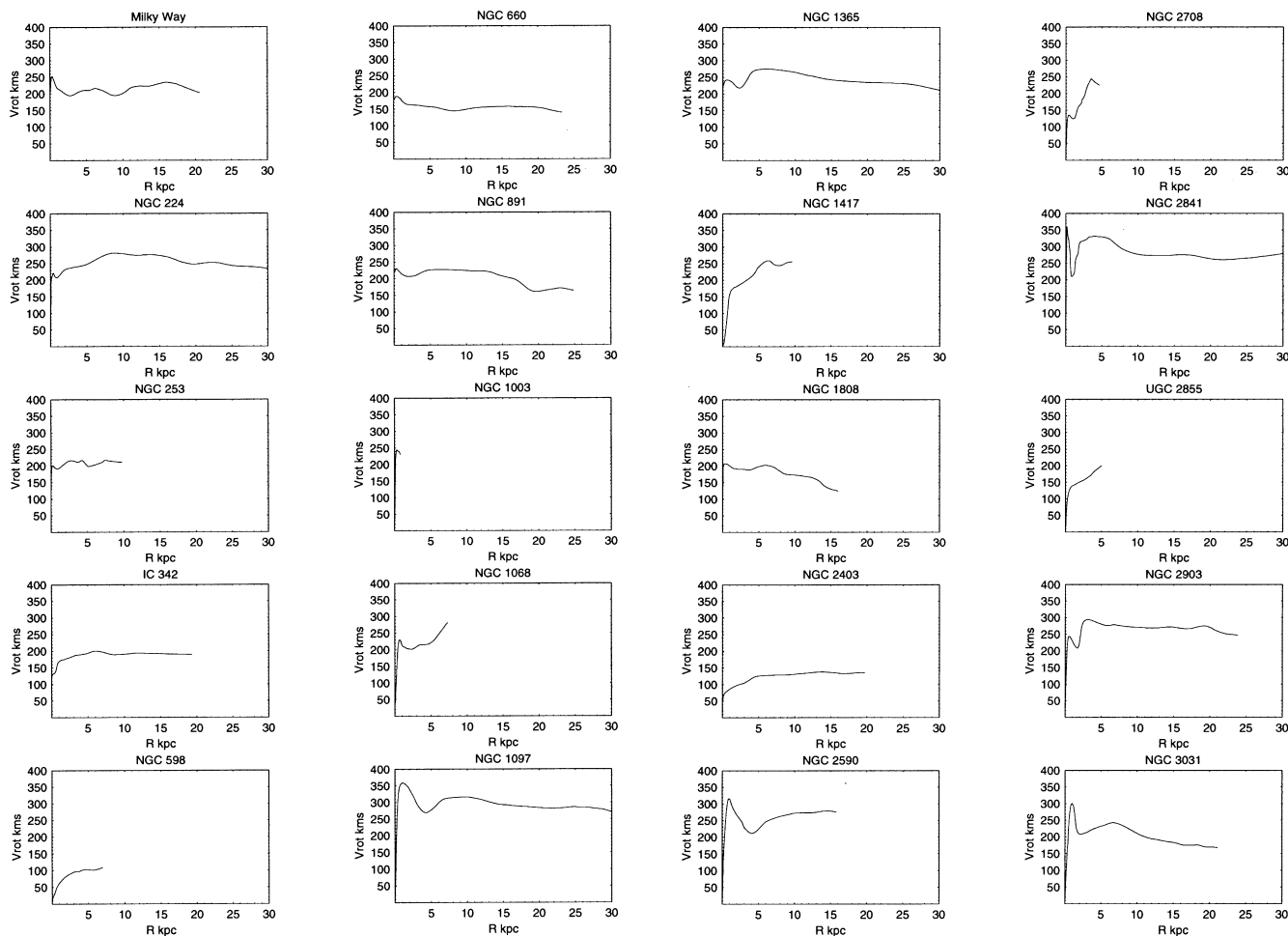


FIG. 10.—Individual rotation curves for spiral galaxies

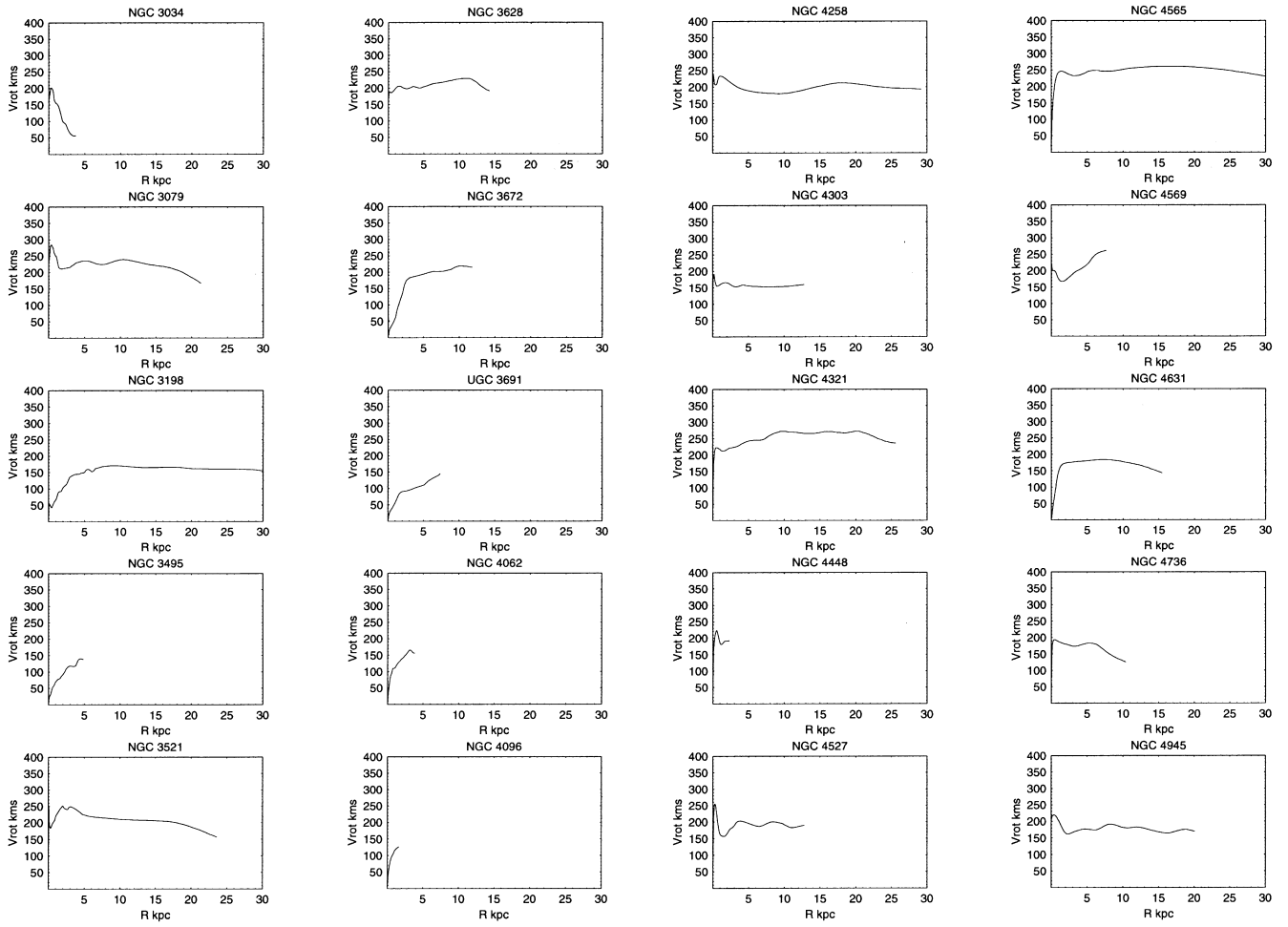


FIG. 10.—Continued

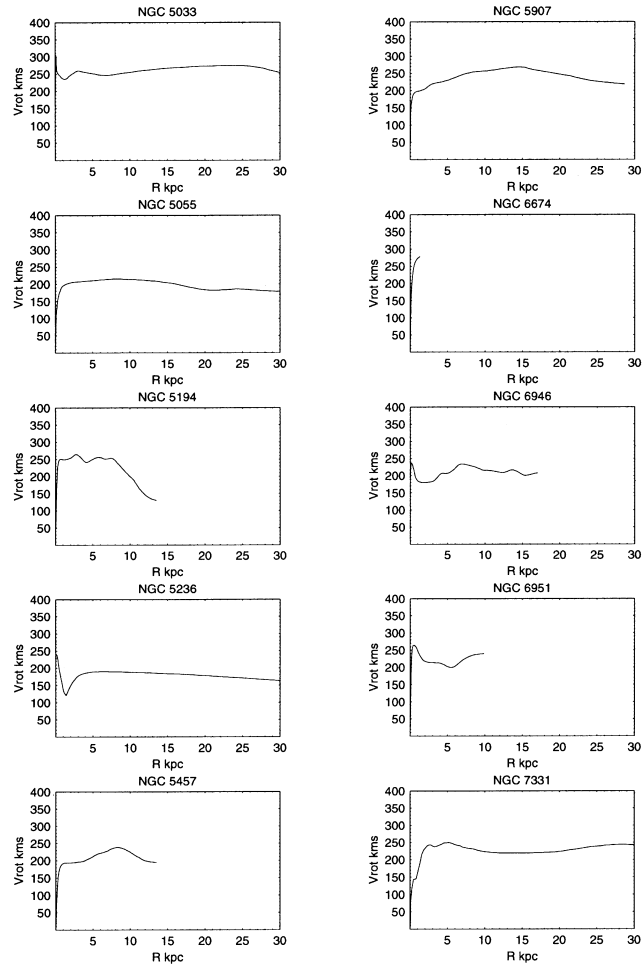


FIG. 10.—Continued

TABLE 1
LIST OF GALAXIES

Name	R.A. (1950)	Decl. (1950)	Type	Activity ^a	Interaction	P.A. (deg)	Inclination (deg)	<i>D</i> (Mpc)	<i>h</i> (kpc)
Milky Way			Sb				90	0	
NGC 224	00 40 00	+40 59 43	Sb			40	77	0.69	5.3
NGC 253	00 45 06	-25 33 40	Sc	SB		51	78.5	2.5	2.3
NGC 598	01 31 02	+30 24 15	Sc			22	54	0.79	2.7
NGC 660	01 40 21	+13 23 25	Sc			45	70	13	
NGC 891	02 19 25	+42 07 19	Sb			19	88.3	8.9	4.2
NGC 1003	02 36 06	+40 39 28	Scd			97	66	9.52	
NGC 1068	02 40 07	-00 13 32	Sb	Sy		79	46	18.1	
NGC 1097	02 44 11	-30 29 01	SBb	Sy		135	40	16	
NGC 1365	03 31 42	-36 18 27	SBb			222	46	15.6	5.8
NGC 1417	03 39 28	-04 51 50	Sb			175	50	54.1	
IC 342	03 41 59	+67 56 26	Sc			40	25	3.9	
UGC 2855	03 43 16	+69 58 46	SBc			112	61	28.77	4.6
NGC 1808	05 05 59	-37 34 37	Sbc	SB		138	58	11.4	
UGC 03691	07 05 11	+15 15 33	Scd			65	65	30.0	
NGC 2403	07 32 06	+65 42 40	Sc			125	60	3.3	2.13
NGC 2590	08 22 29	-00 25 42	Sb			77	71	64.5	2.1
NGC 2708	08 53 37	-03 10 05	Sb			20	68	24.6	
NGC 2841	09 18 36	+51 11 24	Sb			150	68	9	2.3
NGC 2903	09 29 20	+21 43 19	Sc			21	35	6.1	1.9
NGC 3031	09 51 27	+69 18 08	Sb			152	59	3.25	2.5
NGC 3034	09 51 44	+69 55 01	I	SB	yes	71	~90	3.25	
NGC 3079	09 58 35	+55 55 15	Sc	jet		169	~90	15.6	
NGC 3198	10 16 52	+45 48 06	SBc			215	70	9.1	2.5
NGC 3495	10 58 41	+03 53 43	Sd			20	85	12.8	
NGC 3521	11 03 16	+00 14 11	Sbc	LIN		166	75	8.9	2.4
NGC 3628	11 17 49	+13 51 46	Sb/I			104	>86	6.7	
NGC 3672	11 22 30	-09 31 12	Sc			8	67	28.4	
NGC 3953	11 51 12	+52 36 18	SBc			13	54	20.70	
NGC 4062	12 01 31	+32 10 26	Sc			100	68	9.7	
NGC 4096	12 03 29	+47 45 20	Sc			20	73	12.22	
NGC 4258	12 16 29	+47 34 53	Sbc			150	67	6.6	5.6
NGC 4303	12 19 22	+04 45 03	Sc			318	27	8.1	
NGC 4321	12 20 23	+16 05 58	Sc			146	27	15	
NGC 4448	12 25 46	+28 53 50	SBab			94	71	9.7	
NGC 4527	12 31 35	+02 55 44	Sb			66	69	22	
NGC 4565	12 33 52	+26 15 46	Sb			137	86	10.2	5.6
NGC 4569	12 34 19	+13 26 16	Sab	LIN		23	63	8.2	
NGC 4605	12 37 48	+61 53 00	SBc,p			125	69	4.0	
NGC 4631	12 39 40	+32 48 48	Sc/I		yes	86	84	4.30	
NGC 4736	12 48 32	+41 23 32	Sab			108	35	5.1	
NGC 4945	13 02 32	-49 12 02	Sc/I			43	78	6.7	
NGC 5033	13 11 09	+36 51 31	Sc			179	62	14	6.0
NGC 5055	13 13 35	+42 17 39	Sbc			103	55	8	3.8
NGC 5194	13 27 46	+47 27 22	Sc		yes	22	20	9.6	
NGC 5236	13 34 12	-29 36 42	SBc			45	24	8.9	
NGC 5457	14 01 26	+54 35 18	Sc			38	18	7.2	
NGC 5907	15 14 36	+56 30 45	Sc			156	88	11.6	6.0
NGC 6674	18 36 31	+25 19 55	SBb			143	55	42.62	
NGC 6946	20 33 49	+59 58 49	Sc			64	30	5.5	
NGC 6951	20 36 37	+65 55 46	Sbc			154	48	18	
NGC 7331	22 34 47	+34 09 21	Sbc	LIN		167	75	14	4.7

NOTE.—Data are taken from Papers I–IV. The scale radii have been adopted from Kent (1987), van der Kruit & Searle (1982), and Honma & Sofue (1997b).

^a SB: starburst; LIN: LINER; Sy: Seyfert.

REFERENCES

- Bertola, F., Cappellari, M., Funes, J. G., Corsini, E. M., Pizella, A., & Vega Beltrán, J. C. 1998, *ApJ*, 509, L93
- Bosma, A. 1981, *AJ*, 86, 1825
- Casertano, S., & van Gorkom, J. H. 1991, *AJ*, 101, 1231
- Clemens, D. P. 1985, *ApJ*, 295, 422
- Genzel, R., Eckart, A., Ott, T., & Eisenhauer, F. 1997, *MNRAS*, 291, 219
- Ghez, A., Morris, M., Klein, B. L., & Becklin, E. E. 1998, *ApJ*, 509, 678
- Greenhill, L. J., Moran, J. M., & Herrnstein, J. R. *ApJ*, 481, L23
- Honma, M., & Sofue, Y. 1997a, *PASJ*, 49, 453
- . 1997b, *PASJ*, 49, 539
- Kent, S. M. 1987, *AJ*, 93, 816
- . 1991, *ApJ*, 378, 131
- Magorrian, J., et al. 1998, *AJ*, 115, 2285
- Mathewson, D. S., & Ford, V. L. 1996, *ApJS*, 107, 97
- Miyoshi, M., Moran, J., Herrnstein, J., Greenhill, L., Nakai, N., Diamond, P., & Inoue, M. 1995, *Nature*, 373, 127
- Persic, M., & Salucci, P. 1995, *ApJS*, 99, 501
- Persic, M., Salucci, P., & Stel, F. 1996, *MNRAS*, 281, 27
- Richstone, D., et al. 1998, *Nature*, 395A, 14
- Rubin, V. C., Ford, W. K., & Thonnard, N. 1980, *ApJ*, 238, 471
- . 1982, *ApJ*, 261, 439
- Rubin, V., Kenney, J. D. P., & Young, J. S. 1997, *AJ*, 113, 1250
- Sofue, Y. 1996, *ApJ*, 458, 120 (Paper I)
- . 1997, *PASJ*, 49, 17 (Paper II)
- . 1998, *PASJ*, 50, 227
- Sofue, Y., Tomita, A., Honma, M., Tutui, Y., & Takeda, Y. 1998, *PASJ*, 50, 427 (Paper IV)
- Sofue, Y., Tutui, Y., Honma, M., & Tomita, A. 1997, *AJ*, 114, 2428 (Paper III)
- Takamiya, T., & Sofue, Y. 1999a, in preparation
- . 1999b, in preparation
- van der Kruit, P. C., & Searle, L. 1982, *A&A*, 110, 61
- Warner, P. J., Wright, M. C. H., & Baldwin, J. E. 1973, *MNRAS*, 163, 163